



AD-A193 849

ULTRAFINE MICROSTRUCTURE COMPOSITES PREPARED BY CHEMICAL VAPOR DEPOSITION

W. J. Lackey, Garth B. Freeman, Arlynn W. Smith,
John R. Thompson, and Geoving J. Gerard

- Georgia Tech Research Institute

Pradeep K. Agrawal and Woo Y. Lee
School of Chemical Engineering
and

Douglas J. Twait
School of Materials Engineering
Georgia Institute of Technology

216

DTIC
ELECTE
APR 08 1988
S D

Prepared for
Dr. Donald E. Polk
Code 1131
Office of Naval Research
800 North Quincy Street
Arlington, VA 22217-5000

Under
Contract Number N00014-87-K-0036 -

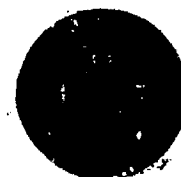
Annual Report for the period January-December 1987

-GEORGIA INSTITUTE OF TECHNOLOGY

A Unit of the University System of Georgia
Atlanta, Georgia 30332



DISTRIBUTION STATEMENT A
Approved for public release
Distribution Unlimited



Annual Report
A-4699-1

ULTRAFINE MICROSTRUCTURE COMPOSITES
PREPARED BY CHEMICAL VAPOR DEPOSITION

W. J. Lackey, Garth B. Freeman, Arlynn W. Smith,

John R. Thompson, and Geoving J. Gerard

Georgia Tech Research Institute

Pradeep K. Agrawal and Woo Y. Lee

School of Chemical Engineering

and

Douglas J. Twait

School of Materials Engineering

Georgia Institute of Technology

Annual Report for the period January-December 1987

Prepared for
Dr. Donald E. Polk
Code 1131
Office of Naval Research
800 North Quincy Street
Arlington, VA 22217-5000

Under Contract Number N00014-87-K-0036

TABLE OF CONTENTS

I. SUMMARY 1

II. INTRODUCTION. 2

III. THERMODYNAMICS. 4

 1. BN + AlN. 4

 2. HfB₂ + SiC. 6

IV. BASIC KINETIC AND TRANSPORT PRINCIPLES AND EQUATIONS. . . 8

V. CHEMISTRY OF CVD OF BORON NITRIDE AND ALUMINUM NITRIDE. .12

VI. MODELS FOR OUR CVD PROCESSES.13

 1. Boundary Layer Model14

 2. Stagnant Layer Model15

 3. Heat Transfer18

VII. FUTURE MODELING EFFORTS19

VIII. COATING EQUIPMENT19

IX. PRELIMINARY EXPERIMENTAL RESULTS.20

X. REFERENCES.22



Accession For	
NTIS CRA&I	<input checked="" type="checkbox"/>
DTIC TAB	<input type="checkbox"/>
Unannounced	<input type="checkbox"/>
Justification	
By <i>per ltr</i>	
Distribution/	
Availability Codes	
Dist	Avail and/or Special
<i>A-1</i>	

ULTRAFINE MICROSTRUCTURE COMPOSITES
PREPARED BY CHEMICAL VAPOR DEPOSITION

I. SUMMARY

It is our goal to develop an analytical model which predicts the experimental conditions which permit the preparation of ultrafine microstructure ceramic composites by chemical vapor deposition (CVD). The model is to be based on classical thermodynamics, mass transport, kinetic, nucleation, and growth theory. The model will be validated for two dispersed phase composite systems. One system will be boron nitride plus aluminum nitride. The other will be hafnium diboride plus silicon carbide. The BN + AlN system is of interest for radomes, windows, and tribological applications while $\text{HfB}_2 + \text{SiC}$ offers potential as a high temperature oxidation resistant material including oxidation protective coatings for carbon-carbon composites.

A thorough literature search was completed for chemical vapor deposition of BN, AlN, and codeposition of dispersed phase composites including $\text{HfB}_2 + \text{SiC}$. The literature on modeling of the chemical vapor deposition process was reviewed. Existing theory applicable to our model is reviewed in this annual report.

Thermodynamic analyses of the BN + AlN and the $\text{HfB}_2 + \text{SiC}$ systems have been completed. These computerized studies indicate that both composite systems can be prepared by codeposition using commercially available, conventional reagents. Results for the $\text{HfB}_2 + \text{SiC}$ system were published.

Mass flowmeters and a pressure control system were purchased and installed on the Georgia Tech CVD System. This equipment permits accurate control of reagent flow rates and total gas pressure. Deposition experiments have emphasized BN, AlN, and codeposition of these two materials to form a dispersed phase composite. Preliminary analysis of the codeposited material by ESCA reveals the desired chemical constituents (B, Al, and N) but more detailed characterization (XRD, SEM, and electron microprobe) is required to verify the existence of the desired dispersed phase composite.

II. INTRODUCTION

Because the properties of composites are frequently superior to those obtainable with single phase materials, it is of interest to explore fabrication of composites by chemical vapor deposition. Multiphase composites have been prepared by chemical vapor deposition by either codeposition, infiltration of fibrous or particulate preforms, or by alternately depositing one or more materials. Our work addresses codeposition of ceramic composites, i.e., simultaneous deposition of multiple phases. In addition to the matrix phase, one or more dispersed phases are present. The shape of the dispersed phase(s) may be spherical, platelike, rodlike (whiskers), or otherwise. We have recently reviewed, in an open literature publication[1], codeposition of dispersed phase composites by chemical vapor deposition.

Several reasons exist for the current high interest in composites. For ceramics, the major thrust is to reduce brittleness, i.e. increase fracture toughness. Extensive progress has been made in improving mechanical properties of particulate, whisker, and fiber reinforced ceramics prepared by chemical vapor deposition and by techniques other than chemical vapor deposition, e.g., powder blending followed by sintering or hot pressing. In addition, silicon carbide whiskers or metal particulates have been added to a wide variety of materials.

Composites which contain a lubricating phase as well as a hard phase (e.g. BN + AlN) offer the promise of tailoring properties such as friction coefficient, hardness, and resistance to wear and erosion. Addition of a hard phase to zinc sulphide or zinc selenide would also be expected to improve the wear and erosion resistance of these important, but soft, window materials. In addition to improved tribological properties, enhanced resistance to oxidation has also been demonstrated for HfB_2 + SiC. This dispersed phase composite has greater resistance to oxidation than either HfB_2 or SiC alone.[1] Electrical, magnetic, optical, and thermal properties can also be favorably influenced by selection of the proper composite system. Deposition of composite coatings is also of interest because of the

possibility of tailoring the coatings thermal expansion coefficient. Increased coating toughness and strength and control of the thermal expansion mismatch between the substrate and coating should contribute to better coating adherence.

A major difficulty in conventional preparation of dispersed phase ceramic or metallic based composites is achieving the desired microstructure, i.e., numerous uniformly dispersed small dispersoid particles. This type of structure is difficult to obtain by melting or by powder blending followed by consolidation since the dispersed particles tend to be too large and they segregate. A further problem, in the case of powder mixtures, is that they tend to be difficult to sinter to acceptably high densities particularly for covalently bonded compounds, such as SiC and Si₃N₄, and for refractory carbides and nitrides and refractory metals in general. One method for circumventing these problems is to utilize heat treatment to cause precipitation of the desired dispersed phase. While this is practical for several metals, unfortunately not many ceramic systems exhibit the required solid solubility. Chemical vapor deposition offers a very versatile process which should be applicable to a large number of matrix-dispersoid chemical combinations. Thus, developing a basic understanding of the interrelationships between processing, structure, and properties of dispersed phase composites prepared by chemical vapor deposition is a worthy objective.

Obviously if the goal is to deposit a multiphase composite, the process conditions must be selected and controlled in order to permit the deposition of the desired phases. As described below, thermodynamic calculations are extremely valuable for this purpose. Reaction kinetics, mass transport, and crystal nucleation and growth are also very important since they influence the microstructure and therefore most properties of the deposit. Important microstructural features for the matrix and dispersed phase are grain size, shape, and orientation. These attributes can be deliberately altered by variation of the process conditions most responsible for influencing reaction kinetics and

crystal nucleation and growth. Progress in modeling the CVD of BN + AlN and HfB_2 + SiC is described in the remainder of this report along with a description of our experimental results on deposition of BN, AlN, and BN + AlN.

III. THERMODYNAMICS

The extensive understanding of the thermodynamics of chemical vapor deposition[2-6] is of great value in predicting the process conditions which should lead to codeposition of the desired solid phases. Computerized calculations predict the equilibrium phases based on minimization of the free energy of all possible gaseous, liquid, and solid species.

We have performed numerous thermodynamic calculations for the BN + AlN and HfB_2 + SiC systems. The calculations were performed using the SOLGASMIX-PV program[7] which we modified in order to permit its use on a personal computer. Results for both chemical systems are summarized below.

1. BN + AlN

The goal of the thermodynamic calculations is to predict reagent concentrations, pressures, and temperatures which will permit codeposition of the desired BN + AlN composite. Also, the information learned about gaseous species assists understanding and modeling of chemical kinetic and mass transport. Composites covering a range of AlN contents are desirable. For example, addition of a small amount of AlN to BN should improve its erosion resistance while additions of BN to AlN should result in better tribological properties because of the lubricating nature of BN.

The thermodynamic calculations were performed for the BCl_3 - AlCl_3 - NH_3 reactant system over the temperature range 1000 to 1700 K. The results were very encouraging in that conditions were found for which it is predicted that BN + AlN can be codeposited. The calculations show that it should be possible to prepare BN + AlN composites which vary in AlN content from 0 to 100%.

A draft report describing the results of the BN + AlN thermodynamic calculations has been prepared. The type of information learned from this study is illustrated by the deposition diagram of Figure 1. This diagram, which resembles, but differs from, a traditional phase diagram shows the equilibrium solid phase(s) as a function of reagent concentration. The region of importance is the two phase region identified as BN + AlN in Figure 1, located near the right side of the composition triangle. Within this region codeposition of BN + AlN is predicted. The composition of the composite varies from 0 to 100% AlN on moving from left to right across the two phase region.

The deposition diagram in Figure 1 is for a specific temperature and total gas pressure (1400 K and 1.0 atm) for the reagent system $\text{BCl}_3\text{-AlCl}_3\text{-NH}_3$. Numerous additional diagrams were constructed in order to evaluate the influence of temperature, pressure, and hydrogen concentration on the codeposition process. For example, the influence of temperature and the ratio of Al to B in the input reactants is given by Figure 2. This graph will be useful in selecting process conditions appropriate for deposition of BN + AlN composites of specific BN contents. Codeposition appears to be feasible over a rather wide range of temperatures (1000-1400 K) and pressures (0.1-1 atm). The calculations also revealed that the deposition efficiency was higher for BN than AlN and that addition of hydrogen increased the deposition efficiency for AlN. Additionally, the influence of partially or completely replacing BCl_3 with B_2H_6 was analyzed. It was learned that both BCl_3 and B_2H_6 , or mixtures, should be appropriate for codeposition of BN + AlN.

The thermodynamic calculations are also valuable in that they give the partial pressures of the numerous gaseous species present during the deposition process. An illustrative plot of pressure versus reactor temperature for the major gaseous species appears in Figure 3. Such plots will be helpful in future kinetic and transport modeling studies and have already been useful in helping us to understand the codeposition process. For

example, the rather high stability (partial pressure) of the AlCl_3 , AlCl_2 and AlCl species accounts for the lower deposition efficiency of AlN compared to BN . This gave us the clue that addition of hydrogen and/or NH_3 to the normal reactant stream would lead to higher AlN deposition efficiencies since their presence would increase the stability of HCl and decrease that of the AlCl_x species. This happens because the source of the chlorine for formation of HCl is the AlCl_x species. Subsequent thermodynamic calculations verified this hypothesis.

2. $\text{HfB}_2 + \text{SiC}$

The dispersed phase composite HfB_2 containing 26 mole percent (20 vol.%) SiC has been shown to have superior resistance to high temperature oxidation and thermal shock than either HfB_2 or SiC alone.[1] For this reason and also because the borides have superior resistance to thermal shock compared to most ceramics, the composite $\text{HfB}_2 + \text{SiC}$ is of interest as a high temperature structural material.[8-11] The material has been prepared by powder blending followed by hot pressing but attempts to prepare coatings of $\text{HfB}_2 + \text{SiC}$, or of the analogous material $\text{ZrB}_2 + \text{SiC}$, by chemical vapor deposition have been unsuccessful.[10,12] The deposits did not consist of the desired phases. Fenter[10] reports that a dense ZrB_2 matrix containing B_4C , instead of SiC , was obtained. The reagents used in that work were ZrCl_4 , BCl_3 , SiCl_4 , and H_2 . The deposition temperature was not given.

In an attempt to learn how to simultaneously deposit the desired $\text{HfB}_2 + \text{SiC}$ composite by CVD, we have studied the thermodynamics of the process. Thermodynamic calculations were performed for the reactant system HfCl_4 , BCl_3 , and CH_3SiCl_3 (methyltrichlorosilane or MTS) again using the SOLGASMIX-PV program. A quantity of hydrogen was added equal to ten times the sum of the number of moles of HfCl_4 , BCl_3 , and MTS present.

The results of the calculations are very encouraging in that, barring kinetic intervention, several conditions were found for which it is predicted that the desired $\text{HfB}_2 + \text{SiC}$ composite

will be deposited. For example, the CVD deposition diagram in Figure 4 shows the solid phases deposited for the $\text{HfCl}_4\text{-BCl}_3\text{-MTS}$ reactant system for a temperature of 1200 K and a total system pressure of 1 atm. The desired region where HfB_2 and SiC codeposit is located near the MTS corner of the diagram. The phase boundaries in Figure 4 were determined by performing the thermodynamic calculation for each of 231 points located within the composition triangle representing all possible 5 mole % increments for the reactants. In order to more accurately define the location of the phase boundaries, calculations were performed at 2 mole % increments for the MTS rich corner of the diagram. The resulting deposition diagram appears in Figure 5. The contour lines within the $\text{HfB}_2 + \text{SiC}$ region of Figure 5 give the mole % SiC predicted for the two phase composite. They show that it should be possible to prepare deposits having a broad range of compositions, including the desired composition of 26 mole % SiC .

It is understandable why previous attempts to codeposit $\text{HfB}_2 + \text{SiC}$ and $\text{ZrB}_2 + \text{SiC}$ were not successful. The point identified as "A" in Figure 4 corresponds to the point which would yield $\text{HfB}_2 + 26$ mole % SiC if the deposition efficiencies were assumed to be the same for hafnium, boron, and SiC . Without benefit of the thermodynamic calculations, this reactant composition would be a logical first choice. The thermodynamically predicted location of the two phase $\text{HfB}_2 + \text{SiC}$ region however, is appreciably shifted to the right (higher MTS concentration) and down (lower BCl_3 concentration) compared to what one might anticipate. Alternatively, perhaps the deposition temperature used in previous experiments was too high.

We have also performed thermodynamic calculations for the purpose of evaluating the influence of temperature and pressure on the codeposition of $\text{HfB}_2 + \text{SiC}$. Briefly, the results predict that codeposition of the desired composite should be possible over the temperature range 1200-1500 K at pressures from 0.1-1.0 atm. Substitution of B_2H_6 for BCl_3 appears feasible. Detailed results of these calculations were presented as an invited paper at the Tenth International Conference on Chemical Vapor Deposition.[1] More recently, additional details were presented.[13]

IV. BASIC KINETIC AND TRANSPORT PRINCIPLES AND EQUATIONS

The purpose of modeling chemical vapor deposition is to relate operating variables (e.g., pressure, temperature, reactant concentrations, reactor geometry, and substrate location and orientation) to performance parameters (e.g., growth rate, uniformity, composition, phase, and microstructure of the composites).[14] Such models can be constructed by describing the underlying principles of kinetics and transport phenomena of CVD processes in terms of solvable mathematical expressions. Generally a set of coupled-partial (or -ordinary) differential equations (i.e., momentum, heat, and mass balances) is required to portray a CVD process realistically.[15] The general forms of these equations which are applicable to most CVD processes are introduced in this section.

Since the film growth rate is slow compared to gas phase dynamics in most CVD reactors, steady state can be assumed. Then the equation of continuity for a fluid element may be written:

$$\nabla \cdot (\rho \vec{v}) = 0 \quad (1)$$

where ∇ = vector differential operator

ρ = total density of the fluid

\vec{v} = mass average velocity of the fluid.

The momentum balance is:

$$\rho \vec{v} \cdot \nabla \vec{v} = \nabla \cdot \bar{\tau} - \nabla P + \rho \vec{g} \quad (2)$$

where \vec{g} = gravitational acceleration

P = pressure.

The viscous tensor for a Newtonian fluid is:

$$\bar{\tau} = \mu [\nabla \vec{v} + (\nabla \vec{v})^T] - \left[\frac{2}{3} \mu \nabla \cdot \vec{v} \right] \bar{I} \quad (3)$$

where μ = viscosity

\bar{I} = unit matrix.

The energy balance takes the form:

$$\rho C_p \vec{v} \cdot \nabla T = \nabla \cdot (k \nabla T) + \sum_{i=1} (\vec{J}_i \cdot \nabla H_i + H_i R_i) \quad (4)$$

where C_p = specific heat

T = temperature

\vec{J}_i = flux of species i relative to the mass average

H_i = partial molal enthalpy

R_i = rate of production of species i due to homogeneous chemical reactions.

The above equation states that convective heat transfer is balanced by a combination of heat conduction and heat generation by inter-diffusion of species and gas phase reactions. The Dufour effect and viscous energy dissipation are neglected since these are known to be small in most CVD systems.[16] Heat evolved from heterogeneous reactions at the substrate surface enters into Eq. (4) as a boundary condition (i.e., constant heat flux at the surface).

The steady state mass balance in the gas phase for species i is:

$$\nabla \cdot \vec{N}_i = R_i \quad (5)$$

where $\vec{N}_i = \vec{J}_i + C_i \vec{v}$

(6)

and C_i is the concentration of species i . The summation of these fluxes is:

$$\sum_{i=1} M_i \vec{J}_i = 0 \quad (7)$$

where M_i is the molecular weight of species i . The flux, \vec{N}_j , can be related to the mole fraction of species i inside the reactor by $(n-1)$ Stefan-Maxwell equations:

$$\nabla x_i = \sum_{\substack{k=1 \\ k \neq i}}^n \frac{x_i \bar{N}_k - x_k \bar{N}_i}{c D_{ik}} \quad (8)$$

where D_{ik} is the binary diffusion coefficient between species i and k and:

$$\sum_{i=1}^n x_i = 1.0 \quad (9)$$

The boundary conditions for Eqs. (8) and (9) are the surface fluxes which are:

$$\bar{N}_i|_{\text{surface}} = - \sum_{m=1}^M S_{im} r_m \quad (10)$$

where S_{im} is a stoichiometric coefficient of species i for heterogeneous chemical reactions, m , with the reaction rate of r_m .

The rates of surface reactions have the general form:

$$r_m = k_m^{-1} [K_m \prod x_i^{S_{im}} - \prod x_i^{-S_{im}}] f(\theta) \quad (11)$$

where $f(\theta)$ is a Langmuir-Hinshelwood expression. This has the general form of:

$$f(\theta) = \frac{1}{1 + \sum_{i=1}^n K_{m_i} (x_i)^q} \quad (12)$$

where K_{m_i} is the equilibrium constant for adsorption and desorption of species i for heterogeneous reaction m . The exponents q and n are determined by the nature of the reaction mechanism.

The net rate of production of each species in gas phase reactions is given by:

$$R_i = - \sum_{n=1}^N S_{in} r_n \quad (13)$$

where S_{in} is a stoichiometric coefficient of species i in homogeneous reaction n . The rate of homogeneous reaction, r_n , has the general form of:

$$r_n = \left[k_n \prod x_i^{S_{in}} - k_n^{-1} \prod x_i^{-S_{in}} \right] \quad (14)$$

where k_n = forward rate constant for homogeneous reaction n
 k_n^{-1} = backward rate constant for homogeneous reaction n

Exact forms of Eqs. (10) through (14) must be determined (or assumed) before attempting to solve Eqs. (1) through (9). The complexity of Eqs. (10) through (14) is governed by kinetics.

Eqs. (1) through (4) become ordinary differential equations (ODE) for one-dimensional analysis and partial differential equations (PDE) for multi-dimensional problems. It is emphasized that solving coupled-nonlinear-PDE systems is a difficult task, if at all possible.

To date, two "sophisticated" models have been developed using this general approach (i.e., simultaneous solution of the above equations) after considerable mathematical simplifications. Rebenne and Pollard[14] have used a finite difference method to solve momentum, heat, and mass equations derived for CVD of boron carbide in an impinging jet reactor. Relatively simple kinetics are assumed for the above modeling purpose. The unique features of their work are that the model: (i) considers deposition of mixed solid phases (e.g., composition and relative amount of carbon and boron-carbon phases) and (ii) includes the largest number of chemical species (e.g., 6 species; BCl_3 , CH_4 , H_2 , BHCl_2 , BCl , and HCl) compared to other CVD models to date. Kinetic parameters such as rate constants are estimated by fitting experimental data available in the literature.

Roenigk and Jensen [17,18] developed a 2-dimensional model for low pressure chemical vapor deposition (LPCVD) of silicon and silicon nitride in a "hot-wall multiple-wafers-in-tube" reactor. This model predicts the effects of operating conditions on the deposition rate at various substrate positions. A numerical method, orthogonal collocation, is used to solve two governing sets of ordinary differential equations (e.g., one for the annulus region and the other for the space between the wafers).

V. CHEMISTRY OF CVD OF BORON NITRIDE AND ALUMINUM NITRIDE

As mentioned earlier, in order to model a multi-reaction system, it is necessary to express each individual reaction step in the forms of Eqs. (11) and (12) for heterogeneous reactions and Eqs. (13) and (14) for homogeneous reactions. For example, Roenigk and Jensen[17] have assumed the following simple kinetic expression for LPCVD of silicon from silane:

$$r_m = \frac{k P_{\text{SiH}_4}}{1 + K_H P_{\text{H}_2}^{1/2} + K_S P_{\text{SiH}_4}}$$

This expression corresponds to a reaction mechanism of: (i) adsorption/desorption equilibria of silane and hydrogen, (ii) no homogeneous reactions, and (iii) rate controlling surface reaction (i.e., surface decomposition of silane). Kinetic parameters k , K_H , and K_S are estimated by fitting experimental data using nonlinear regression. The above expression is only valid at low pressures (ca. 10^{-2} Pa) since it is shown that gas phase reactions (e.g., pyrolysis of SiH_4) take place at higher pressures [19,20].

CVD of silicon is a much simpler and better understood process than that of boron nitride (BN) or aluminum nitride (AlN). However, even for this relatively simple SiH_4 -Si- H_2 system, a mechanism containing 20 intermediate reaction steps has been proposed [21]. Therefore, it is expected that one of the most difficult tasks of modeling CVD of BN, AlN, and BN + AlN is understanding the chemistry of these processes and developing (postulating) possible reaction mechanisms. It seems these mechanisms need to be deduced based on our own experimental data since kinetics of BN- and AlN-CVD have not been thoroughly reported in the literature.

However, our preliminary experimental results have already provided new insights into the adsorption behavior of BCl_3 and AlCl_3 on various substrates. It is observed that BN and AlN can not be deposited on graphite at 1400 K, but they can be deposited on alumina and molybdenum at 1400 K. This behavior is explained in Figure 6. It is not yet sure whether homogeneous reactions

between BCl_3 and NH_3 , which produce stable intermediate species such as $\text{Cl}_2\text{B-NH}_2$ and borazine, take place in the gas phase. Nevertheless, it is suspected that a filled electron orbital (i.e., electron pair donor) existing on nitrogen atoms of either NH_3 or the above mentioned intermediate species favors the Lewis acidic sites (i.e., electron pair acceptor) on alumina as preferential adsorption sites as shown in Figure 6a. Once a monolayer of BN is deposited on the substrate surface, a faster deposition process via nitrogen-to-boron and boron-to-nitrogen adsorptions is expected to proceed as shown in Figure 6b. This postulate is supported by the fact that the hexagonal BN layers are packed directly on top of each other and a boron atom in one layer of these hexagons is located over a nitrogen atom in the next layer.[22] This catalytically enhanced behavior is consistent with experimental observations made by Takahashi et al.[23] They have shown that the deposition rate of BN increases by a factor of 10 when carbon steel substrates are used in the place of alumina due to the presence of catalytically active metallic sites. Obviously, graphite does not contain these acidic sites (see Figure 6c) which are required to facilitate surface reactions (rearrangements or recombinations) into the BN hexagonal structure.

It is interesting to note that BN can, however, be deposited on graphite at higher temperatures (ca. 2000 K).[24] Therefore, it seems that the above described adsorption mechanism is only valid at temperatures around 1400 K. At 2000 K, thermal energy may be large enough to alter the above mentioned electronic interactions.

VI. MODELS FOR OUR CVD PROCESSES

The location and orientation of a flat substrate to be coated in our CVD reactor are schematically shown in Figure 7. In this experimental arrangement, a mixture of reactant gases flows into the furnace cylinder (reaction chamber) and creates the flow pattern (i.e., momentum boundary layer) near the leading edge of the flat substrate in the fluid stream. In addition to

the momentum boundary, a thermal boundary for the gas mixture and a concentration boundary for each gas species develop due to the presence of homogeneous and heterogeneous reactions. Then the objective of modeling is to determine what happens when heat, mass, and momentum are simultaneously transferred across the boundary of the flowing fluid.

Two relatively simple (but realistic) models appear to be promising candidates for this CVD configuration. They are the "boundary layer model" and the "stagnant layer model". Both are based on the boundary layer theory.[15] The stagnant layer model is actually a simplified version of the boundary layer model. A set of ordinary differential equations is required for the stagnant layer model and partial differential equations are necessary to describe the boundary layer model. Details of these models are discussed in this section.

1. Boundary Layer Model

For the boundary layer shown in Figure 7, Eqs. (1) through (4) are simplified to:
continuity:

$$\frac{\partial \rho v_x}{\partial x} + \frac{\partial \rho v_y}{\partial y} = 0 \quad (15)$$

momentum:

$$\rho v_x \frac{\partial v_x}{\partial x} + \rho v_y \frac{\partial v_x}{\partial y} = \frac{\partial}{\partial y} \left(\mu \frac{\partial v_x}{\partial y} \right) \quad (16)$$

energy:

$$\rho c_p v_x \frac{\partial T}{\partial x} + \rho c_p v_y \frac{\partial T}{\partial y} = \frac{\partial}{\partial y} \left(k \frac{\partial T}{\partial y} \right) + \sum_{i=1} (\bar{J}_i \cdot \nabla H_i + H_i R_i) \quad (17)$$

mass:

$$\frac{\partial N_{ix}}{\partial x} + \frac{\partial N_{iy}}{\partial y} = R_i \quad (18)$$

And, Eqs. (6) through (14) remain the same. The boundary conditions, if not stated in Eqs. (6) through (13), are:

$$\text{at } y=0, \quad v_x = 0 \quad (19)$$

$$X_i = X_{i0} \quad (20)$$

$$T = T_0 \quad (21)$$

$$\text{at } y=\infty \text{ or } x \leq 0, \quad v_x = v_{\infty} \quad (22)$$

$$T = T_{\infty} \quad (23)$$

$$X_i = X_{i0} \quad (24)$$

The preceding equations are most general in describing our CVD system. More simplifications can be made by: (i) assuming the physical properties (e.g., ρ, μ, k , etc.) as constants if the thermal gradient is small and (ii) treating v_y as small compared to v_x (i.e., $v_y = 0$) inside of the boundary layer. For a hot wall reactor as ours, no heat flux (i.e., no energy balance and constant physical properties) is often a good assumption as long as heat produced or absorbed from chemical reactions is small.

2. Stagnant Layer Model

Even after all the simplifications, we still have a formidable task of solving the coupled PDE (e.g., Eqs. (15), (16), (18), and the Stefan-Maxwell equations). This difficulty can be avoided by introducing the stagnant layer concept. This assumes that: (i) reactants are not depleted along the axial direction (i.e., constant deposition rate along the axial direction) and

(ii) velocity, thermal, and concentration profiles are the same at any axial position (i.e., no variation in the boundary layers thickness), as shown in Figure 8. This model, therefore, can not predict the deposition rate as a function of the axial direction which may be an important design consideration in industrial applications. However, it is believed that the length (ca. one to three inches) of the substrates used in our experiments is too short for detecting large variations in film thickness.

The governing equations then are:

energy:

$$\frac{d}{dy} \left(k \frac{dT}{dy} \right) + \sum_{i=1} (J_{i,y} \frac{\partial H_i}{\partial y} + H_i R_i) = 0 \quad (25)$$

mass:

$$\frac{dN_{i,y}}{dy} = R_i \quad (26)$$

with Eqs. (6) through (14).

Using this stagnant layer model concept, a very idealized situation for CVD of BN from $\text{BCl}_3\text{-NH}_3\text{-H}_2$ mixtures at typical operating conditions was modeled. The following assumptions were made:

- (i) no thermal energy gradient,
- (ii) mass transfer through the stagnant layer by molecular diffusion only,
- (iii) constant physical properties,
- (iv) decomposition of BCl_3 at the surface is the rate controlling step so the mass transport and surface decomposition of BCl_3 are two competing processes which determine the, overall deposition rate, and
- (v) no gas phase reactions.

With the above assumptions, substitution of Eq. (6) into Eq. (26) gives:

$$J_d = \frac{D_{AB}}{RT} \left(\frac{dP_{\text{BCl}_3}}{dy} \right) \quad (27)$$

where D_{AB} is the diffusion coefficient of BCl_3 in the fluid mixture. The first order approximation of the above equation is:

$$J_d = \frac{D_{AB}}{RT\delta} (P_{BCl_3} - P_{BCl_3}^*) \quad (28)$$

where P_{BCl_3} and $P_{BCl_3}^*$ are the partial pressures of BCl_3 in the bulk phase and at the surface, respectively, and δ is the thickness of the stagnant layer of BCl_3 . From assumption (iv), the rate controlling step is:

$$J_k = \frac{k}{RT} P_{BCl_3}^* \quad (29)$$

The above kinetic expression is derived based on the pseudo first order surface decomposition. At a steady state, the overall growth rate, J_G , is equal to J_d and J_k :

$$J_G = J_k = J_d \quad (30)$$

Combining Eqs. (28), (29) and (30) gives:

$$J_G = \frac{P_{BCl_3}^*/RT}{\delta/D_{AB} + 1/k} \quad (31)$$

The terms δ/D_{AB} and $1/k$ can be thought of as "diffusion resistance" and "kinetic resistance" to the process, respectively. In other words, the process is limited by diffusion if δ/D_{AB} is much larger than $1/k$ and is kinetically controlled if the opposite is true. This simple concept was first introduced by van den Brekel.[25] He combined the above two terms and defined a dimensionless number called the CVD number:

$$CVD \equiv \frac{k\delta}{D_{AB}} \quad (32)$$

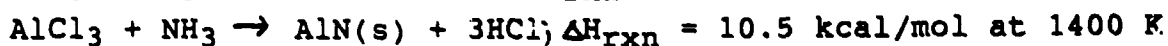
Using the above equations and the physical properties obtained from the thermodynamic correlations given in Reid et al.[26], the CVD number for CVD of BN is calculated to be about 8.5 at the following conditions:

P = 1 atm, T = 1400 K, total flow rate = 650 SCCM
 $P_{\text{NH}_3} = 0.65 \text{ atm}$, $P_{\text{BCl}_3} = 0.04 \text{ atm}$, and $P_{\text{H}_2} = 0.31 \text{ atm}$

The rate constant k is estimated from experimental work of Male and Salanoubat.[27] This result (i.e., CVD number = 8.5) suggests that the overall deposition rate is limited by both diffusion and kinetic steps while the effect of diffusion-resistance is greater. As soon as more experimental data are available, calculations will be extended to account for multi-component diffusion and multi-homogeneous and -heterogeneous reactions.

3. Heat Transfer

As mentioned earlier, the presence of the thermal boundary (or stagnant layer) may play an important role in determining the complexity of mathematics. A preliminary calculation was performed to discern whether or not the "heat transfer effect" is important in CVD of BN and AlN. For this purpose, we have assumed that reactions take place at the surface only. The heats of reaction data were obtained from the Janaf Thermochemical Tables.[28]



As can be seen from the above equations, CVD of BN is an exothermic process so heat is generated at the surface as the reaction proceeds (i.e., constant heat flux at the surface). The equation governing the laminar heat transfer along a flat plate which is at constant heat flux is given by[29]:

$$(T_w - T_\infty)_{\text{avg}} = \frac{q_w L / k}{0.6795 \text{ Re}_L^{1/2} \text{ Pr}^{1/3}}$$

where $(T_w - T_\infty)_{\text{avg}}$ = average temperature difference between the plate and bulk phase over the plate length, L.

Re_L = Reynold's number at the length L

Pr = Prantle's number

q_w = heat flux (ΔH_{rxn} x deposition rate)

From the above equation, the average temperature difference is estimated to be about 32 K at a typical operating condition (ca. growth rate = 1 m/min, 1400 K, 1 atm, total flow rate = 450 SCCM, $X_{\text{BCl}_3} = 0.056$ atm, $X_{\text{NH}_3} = 0.222$ atm, $X_{\text{H}_2} = 0.056$ atm, and $X_{\text{Ar}} = 0.666$ atm). This suggests that the effect of heat transfer may not be neglected in future studies. However, the effect of heat transfer for CVD of AlN is expected to be much smaller than that of BN because of the low AlN deposition rate.

VII. FUTURE MODELING EFFORTS

As mentioned previously, reasonable kinetic mechanisms are required for developing a complete mathematical model. However, the complexity of CVD processes for BN, AlN, and BN + AlN is the biggest obstacle in determining the reaction mechanism associated with these processes. Therefore, a major portion of future experiments will be devoted to understanding the chemistry of these processes (i.e., mainly the effects of reactant concentrations, temperature, and pressure on performance parameters). Also, a numerical algorithm for solving a coupled-ODE system will be constructed and finalized while the above discussed experiments are concurrently conducted.

VIII. COATING EQUIPMENT

An automated system for introducing reagents into the Georgia Tech CVD System was procured. This equipment, which consists of four mass flow meters and a pressure control system, permits accurate control of reagent flow rates and gas pressure. With these modifications the coating system is fully automated and capability exists for conducting controlled experimentation. A mass spectrometer will soon be purchased which will permit sampling and analysis of gases within the coating reaction chamber. This will provide qualitative and quantitative data on gaseous species present within the reactor. This information will greatly assist CVD model development as well as permit independent monitoring of the performance of the reagent supply system.

IX. PRELIMINARY EXPERIMENTAL RESULTS

Fourteen CVD experiments were performed with the intention of depositing BN or AlN or codepositing BN + AlN. The substrate materials employed in these experiments included various shapes of graphite, alumina, fused silica, and silicon nitride. The substrates were suspended by molybdenum wire. The temperature in the reaction chamber was 1400 K for each run. Run condition variables included the rates of reagent gas flow, total gas pressure within the reaction chamber, and the duration of the run. Some deposition resulted in the majority of these experiments. Examination by light microscopy and ESCA is complete but additional characterization is in progress. Most of the samples will be studied by scanning electron microscopy, and selected samples will be analyzed by XRD and the electron microprobe. The following paragraphs are a summary of visual observations and ESCA results.

Four BN deposition experiments were conducted using BCl_3 , NH_3 , H_2 , and Ar as reagents. At one atmosphere pressure a white, uniform coating was obtained on alumina and silicon nitride substrates and on the molybdenum wire. An increase in the NH_3/BCl_3 ratio caused little, if any, change in the appearance of the deposit. The deposit on alumina and silicon nitride became thicker and more translucent in an identical period of run time when the pressure in the reaction chamber was reduced to 0.1 atm. One attempt to deposit BN using the reagents BCl_3 , H_2 , and N_2 was made but no coating was obtained. This indicates that N_2 cannot be substituted for NH_3 as a nitrogen source.

The first two of five AlN deposition experiments produced no coating. The first run was aborted due to clogging of the gas injector. The other experiment which produced no coating may not have had a sufficient amount of AlCl_3 vaporized. The temperature of the vaporizer for that experiment was 146°C. The three subsequent experiments resulted in deposits. The temperature of the AlCl_3 vaporizer was increased to 152°C with a run time of 60 minutes for two of these deposition runs. The best coating

resulted when the temperature of the AlCl_3 was increased to 162°C with a run time of 40 minutes

The first of four BN + AlN codeposition experiments was aborted after 20 minutes due to clogging of the gas injector. A small amount of white material was deposited on the substrates. The ammonia flow rate was reduced and the argon flow was greatly increased in the next experiment, which resulted in a non-uniform, beige colored deposit. "Mushroom" shaped protrusions on the coating were observed using an optical microscope. A more uniform, beige colored deposit which was crystalline in appearance resulted when hydrogen was added to the reagent gas stream in the next experiment. For the last experiment, the flow rates of ammonia and hydrogen were increased and thin beige colored deposits resulted. Examination of these coatings by ESCA revealed about the proper ratios for the B, Al, and N contents. Additional characterization will emphasize determination of the phases present and coating microstructure.

X. REFERENCES

1. W. J. Lackey, Arlynn W. Smith, D. M. Dillard, and Douglas J. Twait, "Proc. of 10th Int. Conf. on CVD," The Electrochemical Society, Inc., Pennington, NJ, 1987, p.1008.
2. G. Eriksson, Acta Chem. Scand. 25, 2651 (1971).
3. G. Eriksson, Chem. Scr. 8, 100 (1975).
4. T. M. Besmann and K. E. Spear, J. Electrochem. Soc. 124, 786 (1977).
5. T. M. Besmann and K. E. Spear, J. Electrochem. Soc. 124 790 (1977).
6. K. E. Spear, "Proc. of 10th Int. Conf. on CVD," The Electrochemical Society, Inc., Pennington, NJ, 1979, p.1.
7. T. M. Besmann, "SOLGASMIX-PV, A Computer Program to Calculate Equilibrium Relationships in Complex Chemical Systems," ORNL/TM-5775, Oak Ridge National Laboratory, Oak Ridge, TN, April 1977.
8. E. V. Clougherty, R. L. Pober, and L. Kaufman, "Synthesis of Oxidation Resistant Metal Diboride Composites," Trans. Met. Soc. AIME 242(6) 1077-82 (1968).
9. Edward V. Clougherty, Edward T. Peters and David Kalish, "Diboride Materials, Candidates for Aerospace Applications," Materials and Processes for the 70's, Vol. 15, National Sampe Symposium and Exhibition, Los Angeles, CA, April-May 1969.
10. John R. Fenter, "Refractory Diborides as Engineering Materials," SAMPE Quarterly 2(3), 1-15, July 1971.
11. J. W. Hinze, W. C. Tripp, and H. C. Graham, "The High-Temperature Oxidation Behavior of a $HfB_2 + 20$ v/o SiC Composite," J. Electrochem. Soc. 122(9), 1249-54 (1975).
12. Personal communication with two industrial firms, March 1987.
13. W. J. Lackey, Arlynn W. Smith, and Douglas J. Twait, "12th Annual Conference on Composites and Advanced Ceramics," The American Ceramic Society, Westerville, OH, 1988 (in-press).
14. H. Rebenne and R. Pollard, J. Am. Ceram. Soc., 70, 907 (1987).
15. R. B. Bird, W. E. Stewart and E. N. Lightfoot, "Transport Phenomena," Wiley & Sons, Inc., New York, 1960.

16. D. W. Hess, K. F. Jensen and T. J. Anderson, Reviews in Chem. Eng., 3, 97 (1985).
17. K. F. Roegnick and K. F. Jensen, J. Electrochem Soc., 132, 448 (1985).
18. K. F. Roegnick and K. F. Jensen, J. Electrochem Soc., 134, 1777 (1987).
19. P. John and J. H. Purnell, Faraday Trans. I., 69, 1455 (1973).
20. J. H. Purnell and R. Walsh, Proc. R. Soc., A293, 543 (1966).
21. M. E. Coltrin, R. J. Kee and J. A. Miller, J. Electrochem. Soc., 131, 425 (1984).
22. E. L. Muetterties, "The Chemistry of Boron and Its Compounds," Wiley & Sons, Inc., London, 1967, p.425.
23. T. Takahashi, H. Itah and A. Takenchi, J. of Crystal Growth, 47, 245 (1979).
24. H. Tanji, K. Monden and M. Ide, "Proc. of 10th Int. Conf. on CVD," The Electrochemical Society, Inc., Pennington, NJ, 1987, p. 562.
25. C. H. J. van der Brekel, Philips Repts, 32, 118, 1977.
26. R. C. Reid, J. M. Prausnitz and T. C. Sherwood, "The Properties of Gases and Liquids," 3rd ed., McGraw Hill Co., New York, 1977.
27. G. Male and D. Salanoubat, "Proc. of 7th Int. Conf. on CVD," The Electrochemical Society, Inc., Pennington, NJ, 1979, p. 391.
28. D. R. Stull and J. Prophet, "Janaf Thermochemical Tables," 2nd ed., National Bureau of Standard, Washington, D.C., 1971.
29. J. P. Holman, "Heat Transfer," 5th ed., McGraw-Hill Co., New York, 1981, p. 192.

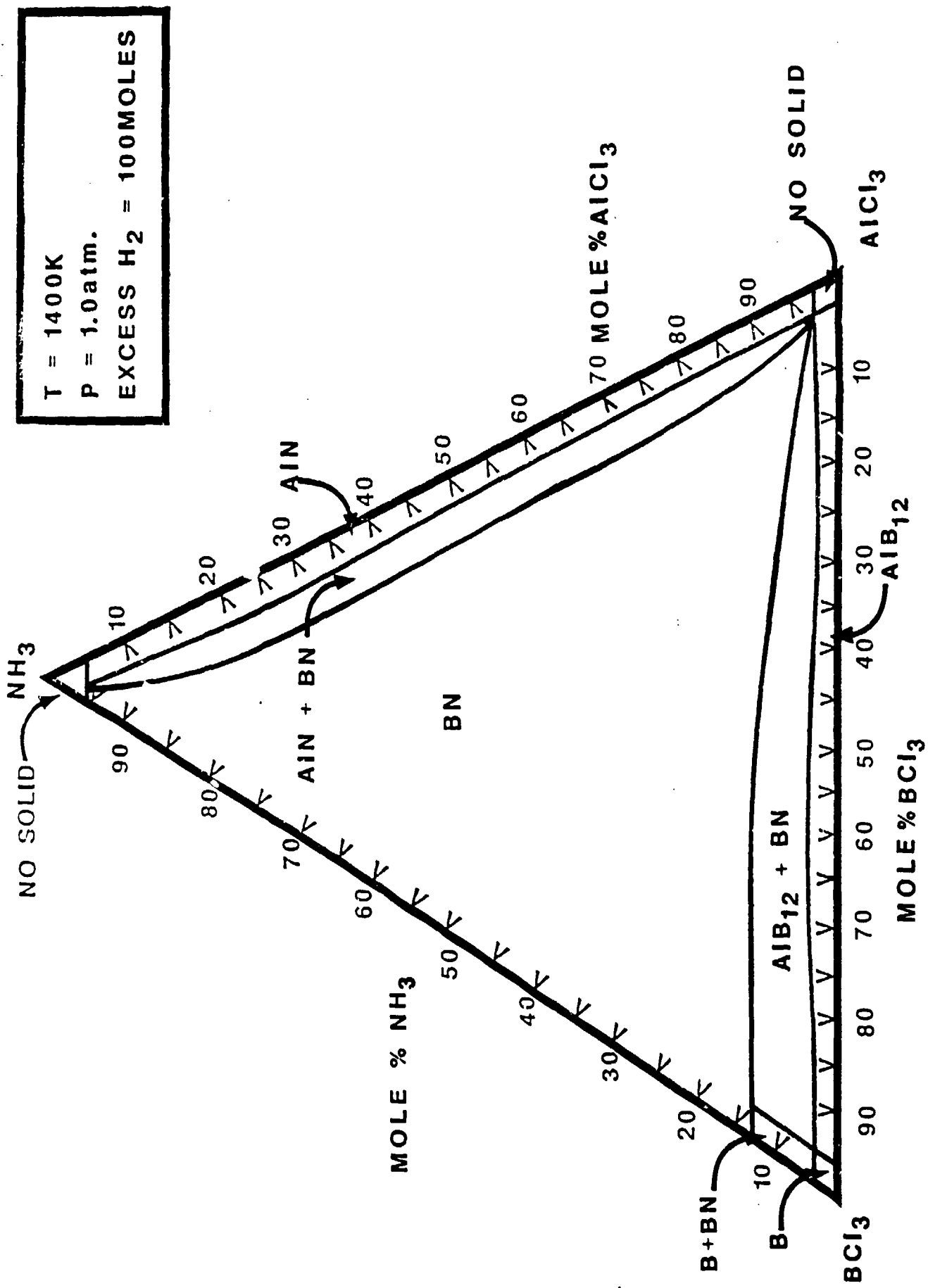


Figure 1. Deposition diagram for the reactant system $\text{BCl}_3\text{-AlCl}_3\text{-NH}_3$ showing a region where $\text{BN} + \text{AlN}$ can be codeposited.

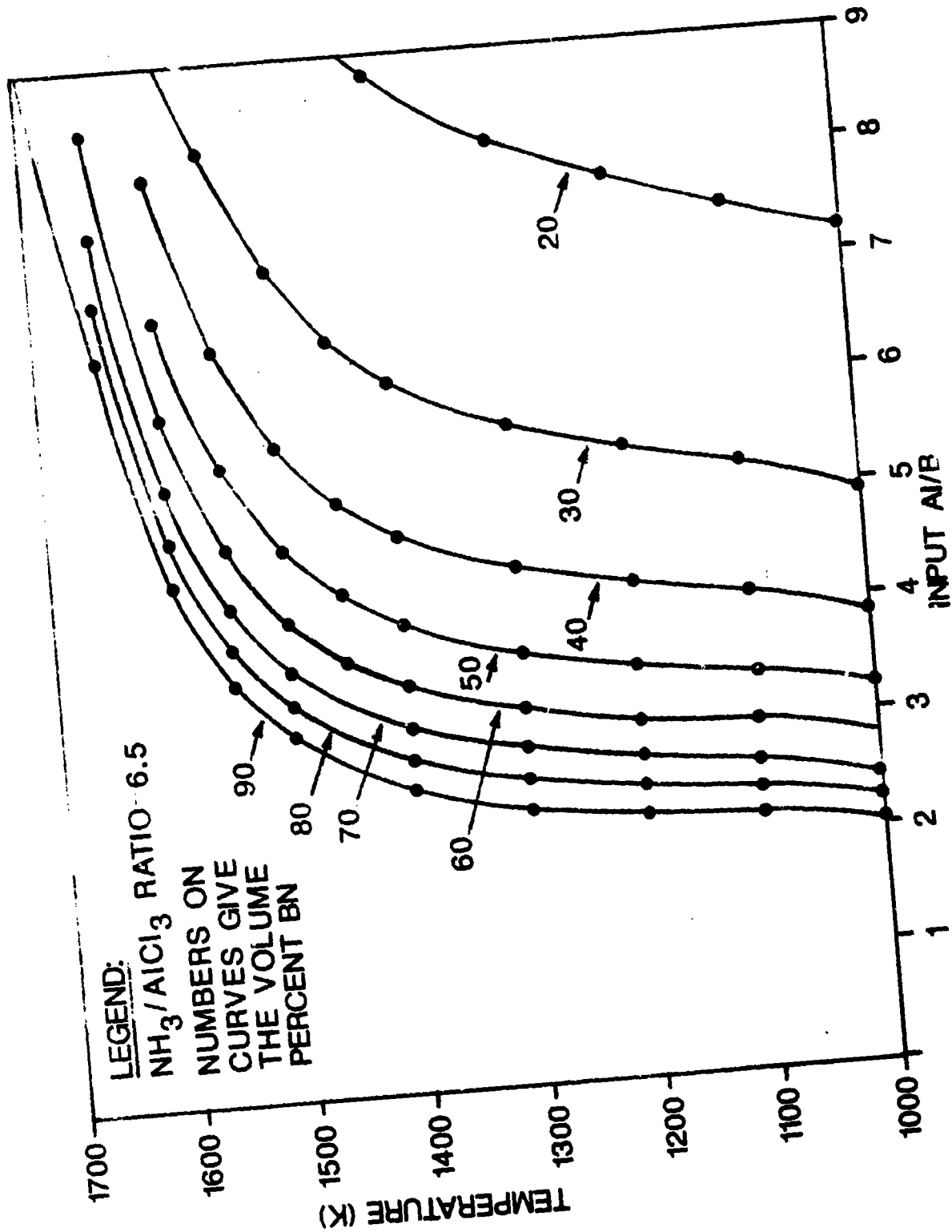


Figure 2. Volume percent BN in BN + AlN composites as a function of deposition temperature and the ratio of Al to B in the input $\text{BCl}_3\text{-AlCl}_3\text{-NH}_3$ reactants. By varying the ratio of AlCl_3 to BCl_3 in the input reagents the composition of the codeposited BN + AlN composite can be varied from 0 to 100% BN.

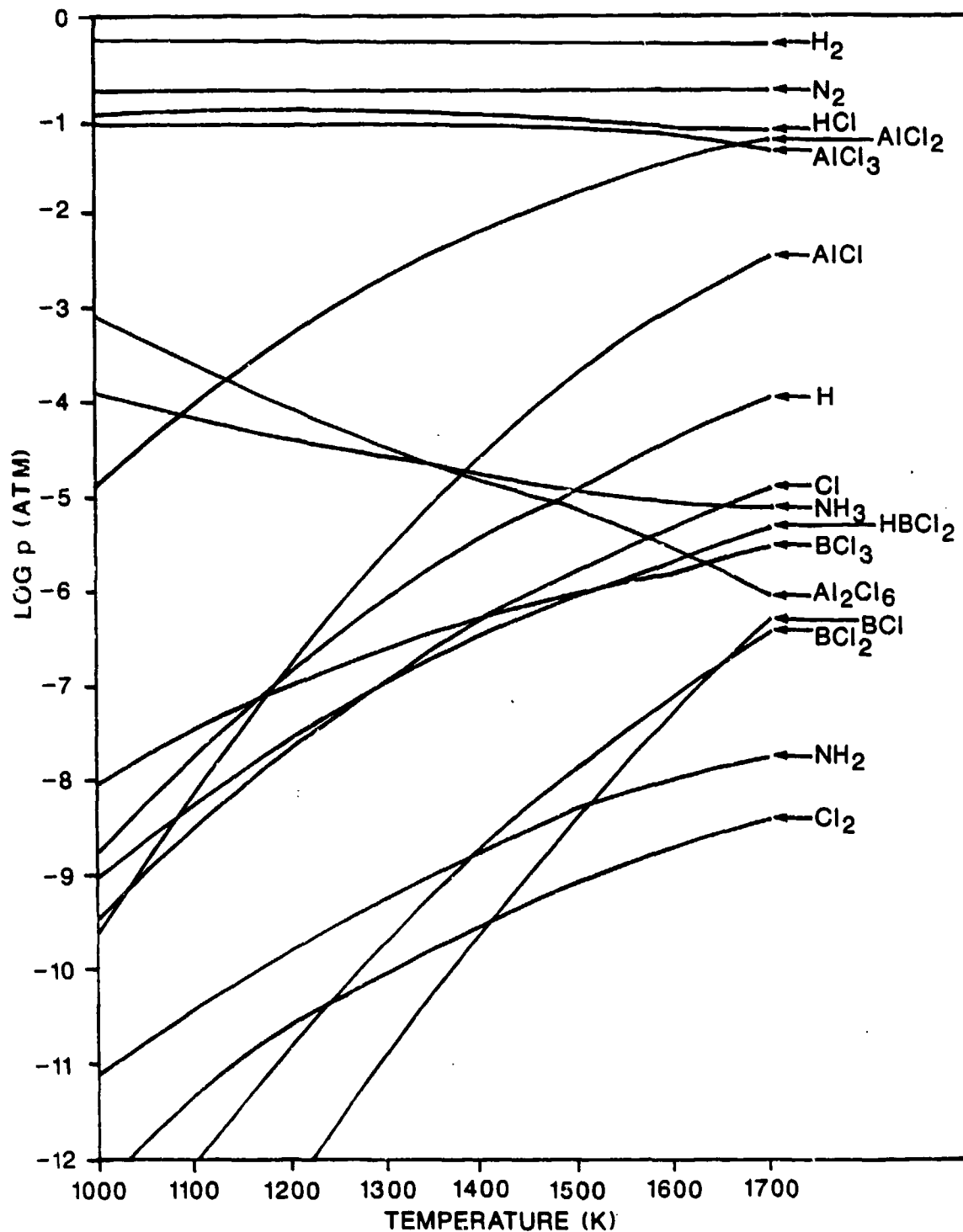


Figure 3. Partial pressures of the major gaseous species as a function of reactor temperature for the reactant system $\text{BCl}_3\text{-AlCl}_3\text{-NH}_3$ which is used for codeposition of $\text{BN} + \text{AlN}$. The relatively high stability of the AlCl_x species compared to species containing boron accounts for the deposition efficiency of AlN being less than that for BN .

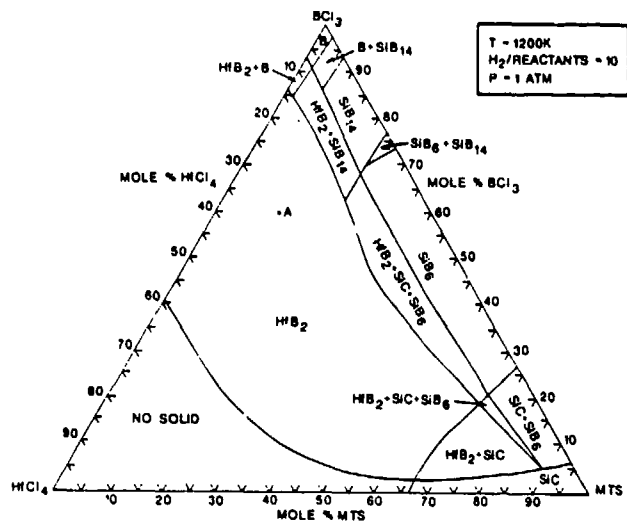


Figure 4. CVD deposition diagram for the reactant system HfCl_4 - BCl_3 - MTS at 1200 K showing region where $\text{HfB}_2 + \text{SiC}$ codeposit.

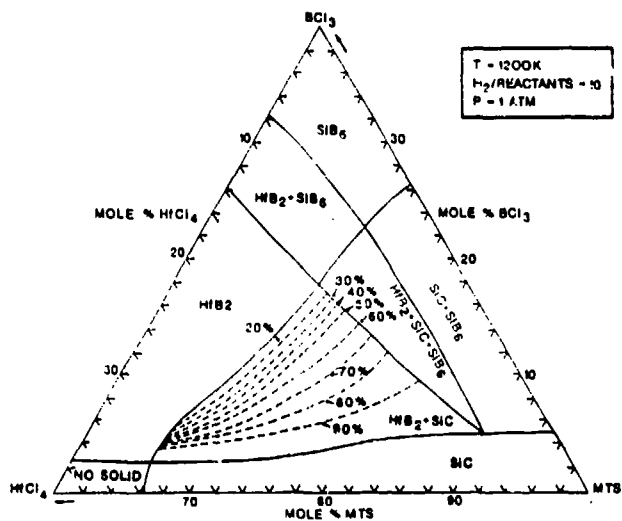


Figure 5. CVD deposition diagram for the reactant system HfCl_4 - BCl_3 - MTS at 1200 K showing mole % SiC contour lines in the two phase region $\text{HfB}_2 + \text{SiC}$.

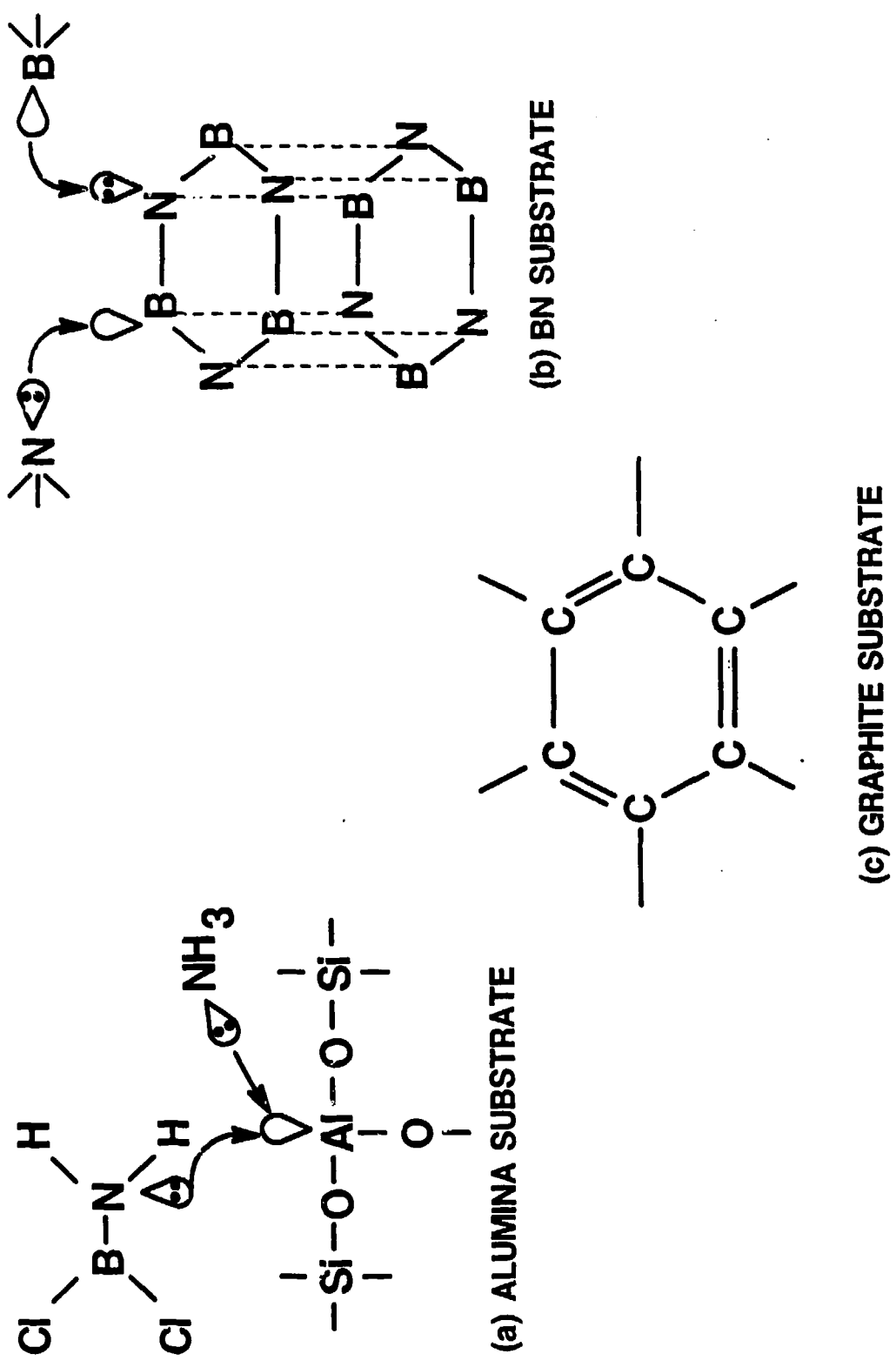


Figure 6. Adsorption behavior of boron containing gas species on various substrates (a) alumina substrate, (b) BN substrate, (c) graphite substrate.

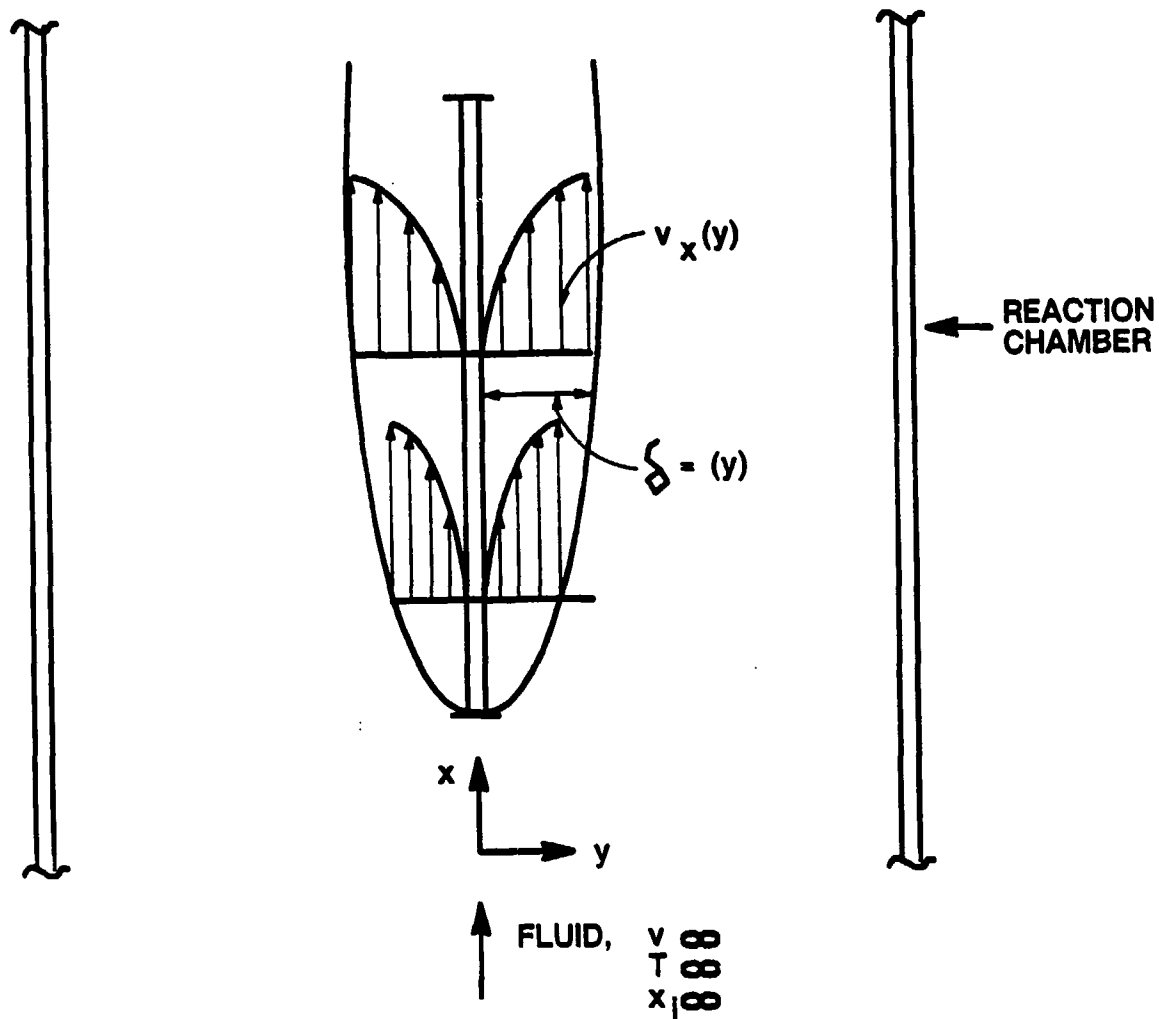


Figure 7. The laminar momentum boundary layer along a flat substrate located inside the CVD reactor.

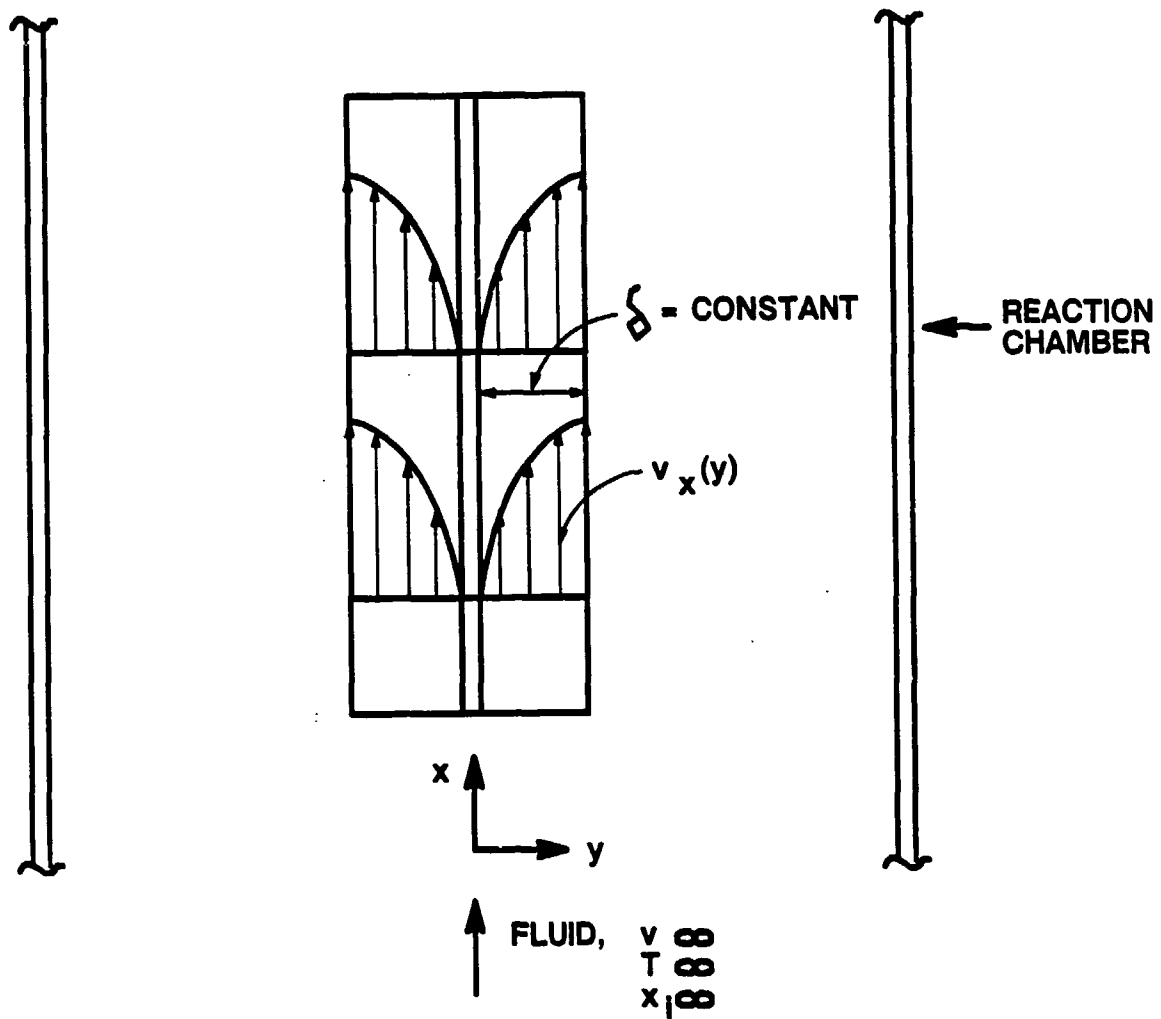


Figure 8. Stagnant layer model.